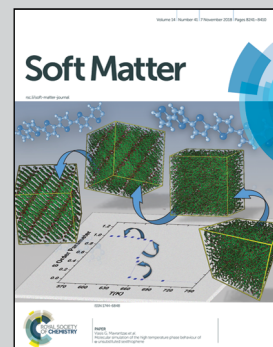


Highlighting research from the Applied Mechanics of Materials Laboratory at Temple University, USA.

Highly efficient fog harvesting on superhydrophobic microfibers through droplet oscillation and sweeping

Superhydrophobic coated microfibers facilitate high-efficient fog harvesting through droplets oscillation, coalescence, and sweeping, driven by the coalescence energy releasing and fog flow.

As featured in:



See Jie Yin *et al.*,
Soft Matter, 2018, **14**, 8276.



Cite this: *Soft Matter*, 2018,
14, 8276

Highly efficient fog harvesting on superhydrophobic microfibers through droplet oscillation and sweeping†

Qiuting Zhang, Gaojian Lin and Jie Yin  *

Water droplet transport on fibers is of great importance for achieving high water collection efficiency from fog. Here, we exploit a new droplet sliding mechanism to accelerate the droplet coalescence and collection for highly efficient fog harvesting by coating hydrophilic microfibers with superhydrophobic layers of assembled carbon nanoparticles. We find that during the initial water collection, unlike the pinned droplets having axisymmetric barrel shapes wrapped around uncoated microfibers, the hanging droplets on coated microfibers with non-wrapping clamshell shapes are highly mobile due to their lower contact hysteresis adhesion; these are observed to oscillate, coalesce, and sweep the growing droplets along the horizontally placed microfibers. The driving force for droplet transport is mainly ascribed to the coalescence energy release and fog flow. After introducing small gravity force by tilting coated microfibers with a small angle of 5°, we find that it can effectively drive the oscillating mobile droplets for directional transport by rapidly sweeping the droplets with a much higher frequency. Finally, the water collection rate from fog on uncoated microfibers over a prolonged duration is found to be improved over 2 times after superhydrophobic coating, and it is further enhanced over 5 times after a small tilting angle of 5°.

Received 16th August 2018,
Accepted 30th September 2018

DOI: 10.1039/c8sm01688g

rsc.li/soft-matter-journal

1. Introduction

Harvesting water from fog is often found in nature on fiber-based structures such as slender leaves of trees, spider webs, and cactus spines.^{1–4} Inspired by such intriguing phenomena, extensive studies have been conducted to replicate the biomimetic features on fiber structures for fog harvesting,^{5–7} which has important potential implications in addressing the challenge of water scarcity in arid regions. Based on the wetting of spider webs, Jiang's group proposed that artificial bioinspired fibers with spindle knots or humps can be harnessed as good water collectors due to their directional transport of tiny droplets and strong hanging ability.^{8,9} Inspired by the cactus spine, researchers found that conical fibers with a curvature gradient and roughness gradient can more efficiently direct the transport of droplets for water harvesting from fog.^{3,10} These studies showed that tuning the geometry and surface structures of the fibers such as surface roughness variation and curvature gradient can induce Laplace pressure difference to overcome the hysteresis adhesion and drive

directional localized transport of tiny droplets to merge into larger ones, which are often pinned to specific sites (e.g., spindle knots or the base of conical wires) for water removal under gravity beyond a critical size.^{11–13} Compared with the removal of accumulated pinned droplets by gravity, a dynamic water droplet transporting process without pinning on fibers can potentially dramatically increase the fog harvesting efficiency due to a potential higher water removal efficiency,^{14,15} which remains largely unexplored.

Here, we propose harnessing superhydrophobic microfibers with a carbon nanoparticle coating for potential high fog harvesting efficiency through dynamic transport of highly mobile droplets. For superhydrophobic curved fiber surfaces, the motion of droplets is much different from the previously reported self-propelled jumping mechanism of droplets on planar superhydrophobic surfaces.^{16–18} The effect of the surface wetting property of microfibers on the process of water collection is investigated through both experiment and numerical simulation including cycles of the static droplet collection and growth, dynamic transport, and successive drop-off of collected droplets. The underlying mechanisms governing the droplet configuration formation and dynamic transport of droplets on fibers are qualitatively revealed through both finite element method-based simulation and theoretical analysis. We found that rather than a symmetric barrel shape wrapped around uncoated

Applied Mechanics of Materials Laboratory, Department of Mechanical Engineering, Temple University, 1947 North 12th Street, Philadelphia, PA 19122, USA.

E-mail: jieyin@temple.edu

† Electronic supplementary information (ESI) available. See DOI: [10.1039/c8sm01688g](https://doi.org/10.1039/c8sm01688g)

hydrophilic microfibers,^{19–22} the droplets on superhydrophobic coated microfibers exhibit an asymmetric clamshell shape hanging on the bottom surface of fibers with a much lower pinning force, making them more prone to transportation. Unlike the previously reported self-propelled jumping mechanism of condensed droplets on superhydrophobic flat surfaces or hydrophobic fibers,^{18,23–25} we observed an effective dynamic sliding transport mechanism on superhydrophobic coated microfibers through droplet oscillation and coalescence along the microfibers driven by the coalescence energy release and environmental perturbation. Finally, the water collection performances over a prolonged duration on both coated and uncoated fibers with different tilting angles were characterized and compared to demonstrate the highly efficient water collection through sliding transport mechanism on coated fibers.

2. Experimental section

Fabrication of superhydrophobic fiber surface

The detailed experimental fabrication process of a superhydrophobic fiber surface is schematically shown in ESI,† Fig. S1a. A glass slide tilted with an angle of 45° was placed in the flame of a paraffin candle. Under it, a silica fiber was held horizontally and rotated continuously to grow assembled carbon nanoparticle-based soots. After growing for 3 minutes, the fiber was homogeneously coated with a layer of carbon nanoparticles.

Characterization of fiber morphology

A SEM Quanta FEG 450 (FEI Co.) scanning electron microscope was used to characterize the surface morphology of fibers in the high vacuum mode and 10 kV acceleration voltage. In Fig. S1b (ESI†), the SEM image shows the detailed morphology of the coating surface with high resolution at 500 nm scale bar.

Characterization of wettability

A Ramé-hart Model 260 Standard Contact Angle Goniometer was used to measure the contact angle of uncoated and coated glass plates at room temperature (22 °C) and relative humidity of 23%. Five μL of deionized water droplets was placed gently onto different sample surfaces. Water contact angles (CAs) were measured by the software. By tilting the sample stage, the contact angle hysteresis was measured at the initial sliding point.

Water collection performance

Fibers were carefully placed horizontally with 90% relative humidity and at 18 at room temperature. The fog flow under the fibers was generated from an ultrasonic humidifier with a velocity of 1.5 m s^{-1} . The tiny droplets with smaller size ($<50 \mu\text{m}$) impacted on the fibers. The optical images of water condensation in the initial stage (Fig. 2) were taken with a Nikon Optiphot-2 Microscope. A high-speed camera with a frame rate of 300 was used to observe the coalescence process within 0.03 s (Fig. S2, ESI†). A Nikon camera was used to record the whole collection process over time.

Simulation of 3-D shape of a droplet on a fiber

The surface energy minimization method implemented in the Surface Evolver (SE) finite element code is used to simulate the 3-D shape of a droplet deposited on a fiber. The total surface free energy (E) associated with the liquid drop with volume V without considering gravity could be expressed as $E = \gamma_{\text{LG}} A_{\text{LG}} + (\gamma_{\text{SL}} - \gamma_{\text{SG}}) A_{\text{SL}} + \iint(\rho g z) \text{d}V$, where g is set to be zero, and γ_{LG} , γ_{SL} , and γ_{SG} represent the interfacial tensions of liquid–gas, solid–liquid and solid–gas, respectively. The boundary conditions at the triple phase contact line include the constant contact angle and no penetration into a rigid cylindrical fiber. At each iteration step, the surface evolver can minimize the total surface free energy E subjected to constraints. The initial shape of simulated condensed water on a fiber is cubic, and it wraps around the fiber. Through continuously minimizing the total surface energy E , the cubic-shaped water droplet evolves to a round shape. The iterations stop until a stable total surface free energy is reached. The perturbation is simulated through moving vertices on the droplet surface a small distance along the direction perpendicular to fiber. After that, the iteration restarts to find the response of droplet shape to the perturbation.

3. Results and discussion

3.1 Wetting on coated and uncoated microfibers

Fig. 1a and b show the scanning electron microscopy (SEM) images of the surface morphology on smooth silica microfibers (diameter of about 150 μm) with and without a coated thin layer of assembled carbon nanoparticles (thickness of about 2 μm). The uniform coating with minimal roughness (Fig. 1b) was generated through a simple flame synthesis process to render the pristine smooth micro-fibers (Fig. 1a) superhydrophobic; the detailed fabrication process is shown in Fig. S1a (ESI†), and carbon nanoparticles with a typical diameter of 30–40 nm were assembled together to form a fractal-like structured surface (Fig. S1b, ESI†).

To characterize the wettability of fiber surfaces, we quantified the contact angle by measuring the advancing (θ_A) and receding contact angles (θ_R) of the single fiber surface through the Wilhelmy method.²⁶ It should be noted that it is challenging to measure the contact angle on a fine curling microfiber surface using the sessile drop method. Fig. 1c and d show the side views of the apparent contact angles on the coated and uncoated fibers during the fog harvesting process. In this process, the fibers were placed in an acrylic chamber with high humidity of 90% and room temperature of 18 °C. The contact angles on the counterpart flat-coated and uncoated surfaces (Fig. 1e and f) through the sessile drop method were reported as 152° and 35°, respectively, which were consistent with our observation of wetting on microfibers. This indicated that carbon nanoparticle coating could dramatically decrease the wettability of fiber surfaces. Fig. 1g shows that the contact angle hysteresis ($\Delta\theta_{\text{hys}} = \theta_A - \theta_R$) decreased from 27° on uncoated fiber to 3° due to the carbon-nanoparticle coating layer. In the following experiments, we have explored harnessing this superhydrophobic fiber coated with carbon nanoparticles for potential highly efficient water collection.

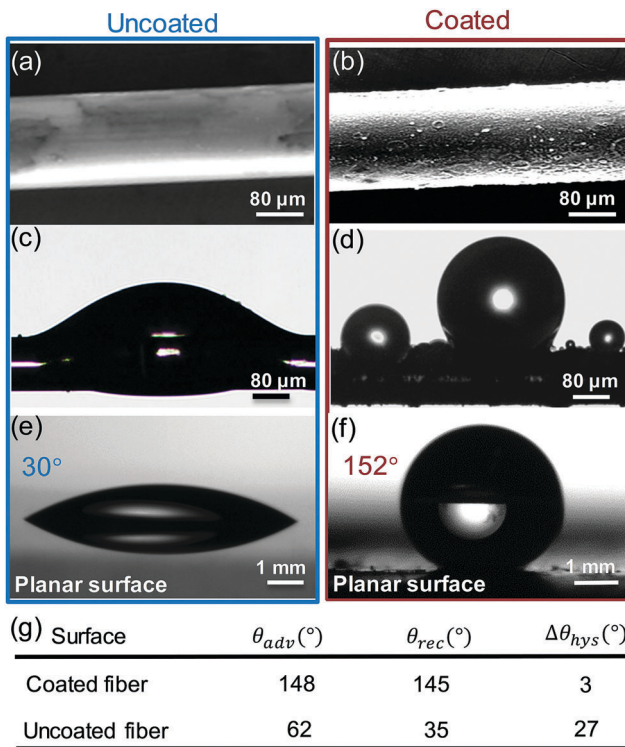


Fig. 1 (a and b) SEM images of surface morphologies on smooth glass microfibers without (a) and with carbon nanoparticle coating (b). (c and d) Apparent contact angles of collected droplets on glass microfibers without (c) and with coated carbon nanoparticles (d). (e and f) Static contact angles of sessile droplets on planar glass surface without (e) and with coated carbon nanoparticles (f). (g) Measured advancing and receding contact angles of coated and uncoated fibers.

3.2 Wetting effect on fog harvesting on microfibers

We first exploited the initial stage of the fog harvesting process on both superhydrophobic (coated) and hydrophilic (uncoated)

fibers under high humidity of 90% at room temperature of 18 °C. Both fibers were placed side by side and horizontally under the microscope for comparison. The fog flow under the fibers was generated from an ultrasonic humidifier with a flow velocity of around 1.5 m s⁻¹. Fig. 2 shows the time-lapse images of the fog impacting process on both fibers captured under an optical microscope at 10× magnification during the first 5 second duration. For the superhydrophobic coated fiber (top), under fog flow impact from the bottom, we observed a dropwise fog harvesting mode with numerous tiny micro-droplets (average diameter less than 20 µm) captured on the bottom of the coated fiber during initial water collection. As more water was collected, the droplets grew larger and coalesced with each other (Fig. 2iv-vi). Similar to the self-removal of microdroplets on superhydrophobic flat surfaces and hydrophobic fibers,^{18,27,28} it was observed that several droplets were jumping away from the superhydrophobic fiber surface due to the surface energy release upon droplet coalescence; however, such a phenomenon occurred only in the initial harvesting period under a low super-saturation condition. As collection further proceeded, the initial nonwetting Cassie–Baxter state transitioned to the flooded Wenzel state under high super-saturation, and its high contact angle was lost. In contrast, the hydrophilic uncoated fiber (Fig. 2, bottom) favored a film-wise water collection mode wrapped around the fiber (Fig. 2ii–iv), which is similar to the observation for hydrophilic planar surfaces. Owing to the Rayleigh instability,²⁹ the water film disintegrated into several individual droplets (Fig. 2v). As the droplets further grew to a larger critical value, the collected water wrapped around the uncoated fiber (Fig. 2vi). Two typical shapes of a droplet on the fibers were proposed by Carroll and Mchall:^{20,22} asymmetric clamshell shape and axisymmetric barrel shape. Here, we observed barrel-shaped droplets wrapped around the uncoated fiber with high wettability, whereas the droplets on the coated fiber exhibited a clamshell shape with a smaller droplet size (Fig. 2vi). During the short duration of fog collection, for both

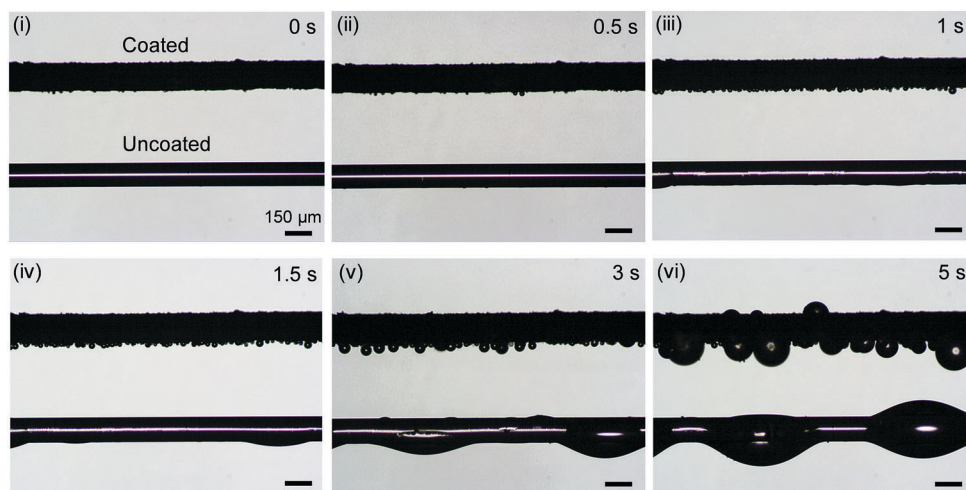


Fig. 2 Time-lapse optical images of the water condensation process on coated and uncoated microfiber surfaces observed under a microscope during the initial 5 second condensation period. On the coated microfiber (top), numerous tiny droplets nucleated and grew, whereas on the uncoated microfiber (bottom), the water film broke into barrel droplets.

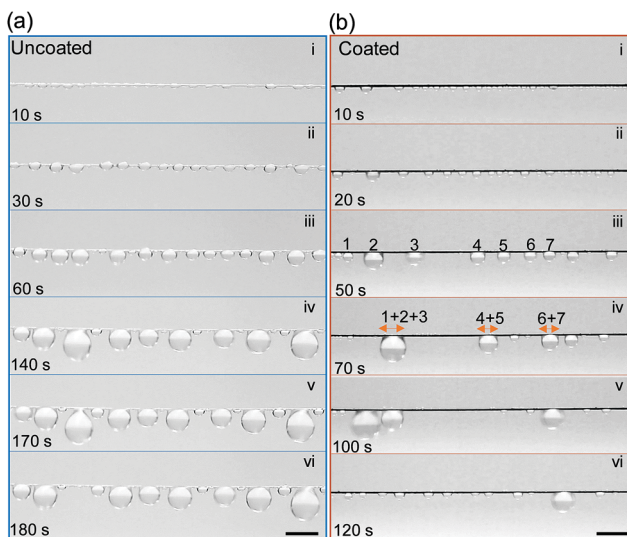


Fig. 3 Time-lapse images of a prolonged duration of water coalescence, transport, and falling process on both uncoated (a) and coated microfiber surfaces (b). Condensed water droplets were pinned on specific sites on uncoated microfibers, whereas they exhibited oscillating and sliding on coated microfibers (scale bar is 2 mm).

fibers, the effect of gravity on the droplet shape was negligible since the droplet size (diameters less than 200 μm and 520 μm for coated and uncoated fibers) was well below the capillary length of water (2.7 mm).³⁰

Next, we investigated the process of accumulation and droplet transport of collected droplets on both coated and uncoated fibers upon prolonged duration of over 120 seconds under high humidity. Fibers with length of 60 mm were fixed horizontally and subjected to a fog flow underneath with a velocity of 1.5 m s^{-1} . The prolonged process of fog harvesting and droplet transport on both uncoated and coated fiber surfaces was captured and recorded by a Nikon camera; the representative time-lapse images are shown in Fig. 3 and dynamic transport processes are shown in the ESI,† Videos S1 (uncoated fiber) and S2 (coated fiber). For uncoated fibers

(Fig. 3a(i)), we observed a series of uniform barrel-shaped droplets at $T = 10$ s. As time increased, the droplets grew larger in size and broke their symmetric barrel shape to hang on the bottom side due to perturbation (Fig. 3a(ii) and (iii)). We also observed that the collected water on the hydrophilic fiber always wrapped around the fiber after growing to a certain volume (Fig. 3a and 4a). Further moisture exposure led to coalescence of neighboring droplets (Fig. 3a(iv)) to form relatively large-sized droplets, which were pinned on their specific sites (Fig. 3a(iv)–(vi)). Finally, the large-sized droplets were removed by gravity by overcoming the capillary adhesion (Fig. 3a(vi)).^{31,32}

The critical maximum droplet size of a stationary droplet before detaching can be predicted based on the balance between the gravity and capillary adhesion force given as

$$\rho g V = 4\pi b\gamma \cos(\pi/2 - \beta) \quad (1)$$

where ρ and γ are the water density and surface tension, respectively, b is the fiber radius and β characterizes the asymmetric degree biasing from the center of the fiber. Therefore, the maximum hanging radius on the uncoated fiber can be ideally calculated as 1.1 mm with β approaching $\pi/2$ and a fiber radius of 75 μm , which is slightly larger than the measured value of 0.95 mm at $T = 170$ s in experiments. A larger fiber radius can increase the hanging drop size (Fig. S2, ESI†).

In contrast, rather than the hydrophilic uncoated fibers having stationary droplets, the superhydrophobic coated fiber favored a dynamic sliding transport of collected droplets along the fiber. Unlike the hanging droplets wrapped around the uncoated fiber, we observed that as fog impacted the bottom, the collected water droplets on partially wetted coated fibers always hang on the bottom of the fiber without wrapping the fiber on the top even for a large volume of droplets (Fig. 3b and 4a). This was evidenced by the fact that a few water droplets could still condense on the top of the coated fiber with a lower saturation state (Fig. 4a). This could lead to a much lower pinning force due to the relatively smaller contact area when compared to that of

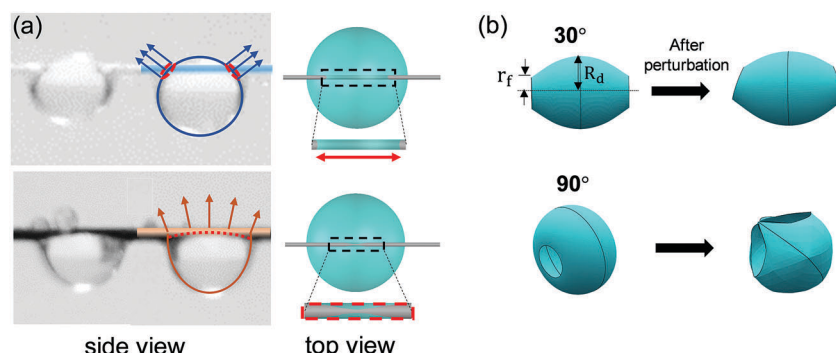


Fig. 4 (a) Side and top schematic views of condensed water droplets on uncoated (top) and coated (bottom) microfibers. Red dashed lines represent triple phase contact lines with different directional adhesion forces. (b) The simulated equilibrium conformations of axial-symmetric barrel-shaped droplets on fibers with contact angles θ being set to 30° and 90° (left) to represent hydrophilic and superhydrophobic wetting states on fibers. After perturbation, the barrel shape becomes asymmetric on hydrophilic fibers, whereas it transitions to an unstable hanging clamshell shape on superhydrophobic fibers (right).

hydrophilic fibers. At $T = 50$ s, droplets with an average radius of 0.6 mm started oscillating randomly and coalescing sequentially (Fig. S3, ESI[†]). We believe that external perturbations such as vibration, air flow, and interaction of water droplets could eventually propel the initial movement of droplets along the fiber. After that, during the process of horizontal oscillation, the oscillating droplets merged with neighboring tiny drops to form a larger size and released coalescence energy to maintain transporting of the droplets. During this process, coalescence of the droplets could efficiently clean up the fiber surface through sweeping. Unlike pinning of droplets on a specific site of the uncoated surface, the first detached droplet on the coated fiber was collected at an earlier time of 100 s due to dynamic oscillation and sliding.

Furthermore, to examine the effect of the fog flow rate on the water collection performance on microfibers, we largely decreased the velocity of the fog flow rate from 1.5 m s^{-1} to 0.5 m s^{-1} in the setup acrylic chamber with 90% humidity. We found that the water collection performance of the coated microfiber largely decreased due to two major contributing factors. One is the decreasing number of tiny droplets impacted on the fibers per second for potential water collection source; the other is the smaller perturbation force generated from a relatively lower air flow rate, which leads to slower oscillations of droplets. Under a slow fog flow rate of 0.5 m s^{-1} , for the coated fibers (Video S3, ESI[†]), we observe that the water droplets on coated fibers oscillate in a smaller range and with a lower frequency, resulting in lower efficiency of coalescence of droplets. In addition, the droplets require more time to grow due to the reduced number of impacted small droplets on the microfibers during a slow fog flow. For uncoated microfibers (Video S4, ESI[†]), since the perturbation of air flow has no effect on the stable pinned droplets, the reduced water collection performance is mainly due to the smaller number of impacted droplets on microfibers.

3.3 Theoretical and numerical insights on fog harvesting performance on microfibers

To better understand the underlying mechanism of droplet sliding on a superhydrophobic fiber surface, we qualitatively analyzed the conformation change of hanging droplets under perturbation through finite element simulation in the absence of gravity (please see experimental method for more information). Under an idealized condition, the droplet at equilibrium adopted an axial symmetric barrel shape and its shape was solely determined by the contact angle θ . Here, we chose $\theta = 30^\circ$ and 90° to represent the hydrophilic and superhydrophobic wetting states on the fibers, respectively. It should be noted that for an axial-symmetric barrel-shaped droplet wrapped around a cylindrical fiber, $\theta = 90^\circ$ is the maximum contact angle and represents the superhydrophobic state on a fiber. Fig. 4b shows the simulated equilibrium conformations of hanging droplets on a fiber of radius r_f with $\theta = 30^\circ$ (top) and 90° (bottom). Both droplets exhibited an axial-symmetric barrel shape, which could be characterized by the normalized droplet size R_d/r_f and the contact angle θ (top of Fig. 4b). To determine if the equilibrium conformations

were stable, we applied slight perturbation to the droplet at equilibrium by moving vertices of the droplet surface downward along the direction perpendicular to the fiber with a small distance of 1/10 of the fiber radius to qualitatively simulate the possible perturbation in experiments (Fig. S4, ESI[†]). As we can see, such perturbation broke the axial symmetry of the droplet. For droplets with $\theta = 30^\circ$, the water droplet still wrapped around the fiber with a relatively larger volume underneath the fiber. In contrast, for droplets with $\theta = 90^\circ$, once slight perturbation was applied, the whole water droplet tended to move to one side with only a singular point connected to the fiber, as shown in the simulation, indicating that the axial symmetric barrel-shaped droplet on the superhydrophobic fiber was highly unstable. Therefore, in experiments, external perturbations such as vibration, air flow, and interaction of water droplets could eventually lead to an asymmetrical conformation on superhydrophobic coated fibers. The stability of hanging water droplets having a barrel shape on fibers was theoretically studied by Carroll;¹⁹ he found that a barrel-shaped water droplet hanging on a fiber required normalized radius R_d/r_f to be infinite to ensure a stable barrel shape, which does not exist physically.

The one-side hanging of a water droplet could potentially lead to a much higher mobility of water droplets on fibers when compared to that of the droplets wrapped around the fiber. For the water droplets wrapped around the uncoated fiber, two segments of circular triple phase contact line (highlighted with red circles in Fig. 4a) could provide a larger horizontal component of the adhesion force. For the one-side hanging water droplet, the horizontal component of the adhesion force was much smaller compared to that for the droplet wrapped around the fiber since the normal direction of the points on the triple phase contact line is mostly perpendicular to the fiber (bottom of Fig. 4a). Therefore, based on the above analysis, it can be demonstrated that it is much easier for the droplet on a superhydrophobic coated fiber to keep sliding with the release of coalescence energy.

With the lower contact hysteresis adhesion on superhydrophobic coated fibers, we further explored the potential fog harvesting ability at a small tilting angle of 5° for gravity-driven directional transport, and we compared it with that on uncoated fibers. Fig. 5 shows that similar to the case of horizontal fibers, droplets wrapped around and remained stuck on the tilted uncoated hydrophilic fiber against gravity (Video S5, ESI[†]). However, by applying a gravity force, droplets on the coated fiber could effectively overcome the resistance and slide downward along the fiber with a higher dropping frequency (Video S6, ESI[†]). In this situation, the critical condition for the drop to slide on the fiber should satisfy the following equation:

$$F_r = \rho g V \sin \alpha \quad (2)$$

Here, F_r represents the force required to move a stationary droplet resulting from surface tension and the contact angle hysteresis, and the right term represents the driving force from the gravity with a tilting angle α . This required moving force has been previously presented by Mead-Hunter *et al.*³³ with

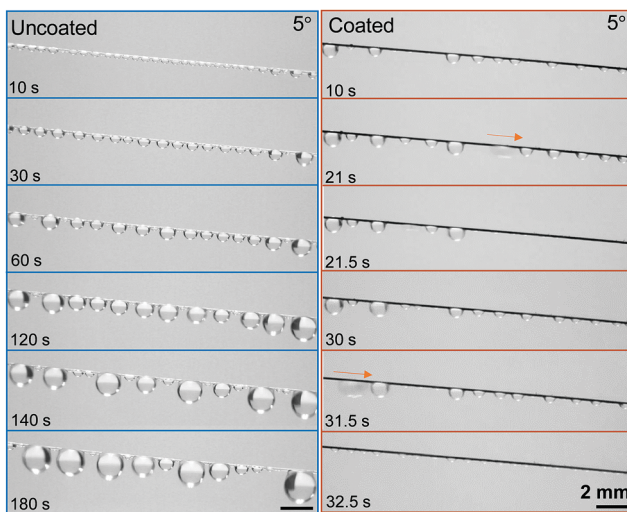


Fig. 5 Time-lapse images of the water capture process on both uncoated (left) and coated microfiber surfaces at a small tilting angle of 5° (right). The droplets on an uncoated fiber remained pinned on specific sites without sliding. First, maximum-sized hanging droplets detached from the microfiber at 180 s (left), whereas a faster collection rate was observed on coated microfibers with droplet sliding and sweeping. (right).

$$F_r = 2\pi r\gamma \left(\int_0^{2\pi} \cos \theta_A \hat{v} d\varphi + \int_0^{2\pi} \cos \theta_R \hat{v} d\varphi \right) \quad (3)$$

where \hat{v} is a normalized vector related to droplet shape, r is the radius of the contact line, θ_A and θ_R represent the advancing angle and receding angle, respectively,³⁴ and φ is the angular position on the contact line around the fiber. Since the coated fiber surface had a much lower water contact angle hysteresis (the difference between advancing angle and receding angle)^{35,36} compared with the hydrophilic surface, a small external force produced by gravity could easily drive the droplets to slide forward by overcoming the smaller horizontal component of the contact hysteresis adhesion force; the water droplets remained pinned to the uncoated fiber despite their large increasing size due to the much larger resistance force until their drop-off under gravity when beyond the critical volume in eqn (1). Therefore, we

observed that the coated fiber exhibited much better performance on water removal efficiency. At $T = 21$ s and 31.5 s, the first and second critical drops on the coated fiber swept all the other drops ahead of them in one transport process within a short period of 0.5 s. After that, new small droplets were collected sequentially and grew on the swept region, which could strongly enhance the water collection efficiency. In contrast, for the uncoated hydrophilic fiber, the detachment of the first drop required a much longer time of 180 s until it grew to the maximum hanging volume. Therefore, the droplet dynamic transport process on the superhydrophobic coated fiber dominated overall fog harvesting by inducing a higher falling frequency compared with the gravity-driven detachment of pinned droplets on specific sites on uncoated fibers.

3.4 Water collection efficiency on microfibers

To quantitatively evaluate the water collection efficiency on fibers, we further investigated the fog harvesting process for a prolonged duration with all conditions unchanged. Fig. 6a shows the comparison of the water collection volume per length between coated and uncoated fibers with and without tilting as a function of collection time over a relatively short period of 5 minutes. For all the studied fibers, the water collection volume approximately increased linearly with the collection time, the slopes of which were almost the same for both horizontal coated and uncoated fibers, whereas the slope for coated fibers was slightly larger than that of uncoated ones after tilting. Specifically, for horizontal fibers, the volume of collected water at $T = 5$ min from the coated fiber was over $134 \mu\text{L}$, which was twice as large as the volume collected by the uncoated one. Each dot in the figure represents the collection of one more droplet after detaching from the fibers. Compared to the result for uncoated fibers, the volume of collected water at $T = 5$ min on both coated and uncoated tilted fibers ($\alpha = 5^\circ$) nearly doubled. The reason is that for coated fibers, rather than pinning and drop-off, water droplets could slide directionally along the fiber driven by the combination of coalescence energy release and gravitational force. This sliding mechanism led to a much higher falling frequency, as demonstrated by the dense

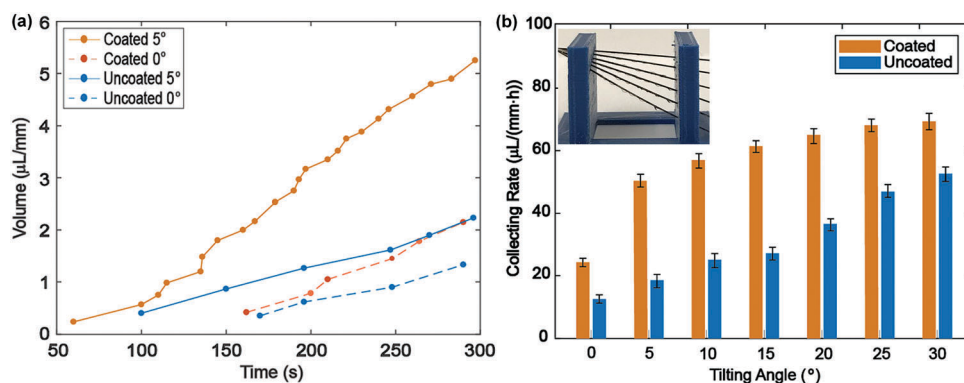


Fig. 6 (a) Experimental results of the water collection volume over 5 minutes on coated and uncoated microfibers with and without slight tilting (tilting angle is 5°). (b) Comparison of measured water collection rates over a prolonged duration of 5 hours on coated and uncoated microfibers with various tilting angles.

points in the brown dashed line. The water collection volume dramatically improved by 158% to 320 μL on the coated surface at $T = 5$ min, suggesting an effective way of harnessing nonwetting fiber surfaces for enhanced water collection rates due to a higher falling frequency. The water collection performances of fibers with various tilting angles over a much longer duration of up to 5 hours were further compared, and the results are summarized in Fig. 6b; the inset shows a fiber array with tilting angles changing from 5° to 30° . This showed that compared to a gradual increase on uncoated fibers, the water collecting rate on repellent fiber surface increased dramatically by more than two times at smaller tilting angles (5°) but then plateaued at larger tilting angles. The primary contribution to the observed distinction of collecting rates between coated and uncoated fibers was the different contact hysteresis adhesions. For coated fibers, the hysteresis contact angle was measured as 3° , which indicated that due to small-angle oscillations, droplets could immediately sweep through the whole fiber surface, and further increase in the tilting angle exhibited negligible effects. In contrast, due to higher hysteresis adhesion (27°) on uncoated fibers, no significant sweeping behavior was observed for uncoated fiber with the highest tilting angle up to 30° . The droplet coalesced with the next lower one and stopped at a lower point; therefore, the collecting rate increased gradually. Generally, the fog harvesting rate could be improved by the superhydrophobic surface coating, especially at slightly tilted angles.

4. Conclusion

In conclusion, we demonstrate that by coating hydrophilic microfibers with superhydrophobic layers of assembled carbon nanoparticles, the water harvesting efficiency for horizontal microfibers from fog can be largely improved over two fold. The introduction of a small tilting angle of 5° to the coated microfibers can further increase the water collection rate over three fold through directional transport and sweeping along the microfiber. One main contributing factor is that the lower contact hysteresis adhesion on the coated microfiber leads to a non-wrapping clamshell shape of droplets, which could result in a sliding mechanism to accelerate the coalescence and sweeping efficiency. Under slight perturbations from the environment such as air flow and vibration, faster droplet falling frequency can help improve the water collection rate. This study provides an important strategy of harnessing superhydrophobic coatings on a curved fiber surface for potential water harvesting over large areas with a higher collection efficiency.

Conflicts of interest

There are no conflicts of interest to declare.

Acknowledgements

J. Y. acknowledges the funding support from the start-up at Temple University and National Science Foundation (NSF-CMMI-1745921).

References

- 1 E. B. Limm, K. A. Simonin, A. G. Bothman and T. E. Dawson, *Oecologia*, 2009, **161**, 449–459.
- 2 Y. Zheng, H. Bai, Z. Huang, X. Tian, F.-Q. Nie, Y. Zhao, J. Zhai and L. Jiang, *Nature*, 2010, **463**, 640.
- 3 J. Ju, H. Bai, Y. Zheng, T. Zhao, R. Fang and L. Jiang, *Nat. Commun.*, 2012, **3**, 1247.
- 4 A. Roth-Nebelsick, M. Ebner, T. Miranda, V. Gottschalk, D. Voigt, S. Gorb, T. Stegmaier, J. Sarsour, M. Linke and W. Konrad, *J. R. Soc. Interface*, 2012, **9**, 1965–1974.
- 5 K.-C. Park, S. S. Chhatre, S. Srinivasan, R. E. Cohen and G. H. McKinley, *Langmuir*, 2013, **29**, 13269–13277.
- 6 Z. Songnan, H. Jianying, C. Zhong and L. Yuekun, *Small*, 2017, **13**, 1602992.
- 7 F. T. Malik, R. M. Clement, D. T. Gethin, W. Krawszik and A. R. Parker, *Bioinspiration Biomimetics*, 2014, **9**, 031002.
- 8 H. Bai, X. Tian, Y. Zheng, J. Ju, Y. Zhao and L. Jiang, *Adv. Mater.*, 2010, **22**, 5521–5525.
- 9 Y. Hou, Y. Chen, Y. Xue, Y. Zheng and L. Jiang, *Langmuir*, 2012, **28**, 4737–4743.
- 10 J. Ju, K. Xiao, X. Yao, H. Bai and L. Jiang, *Adv. Mater.*, 2013, **25**, 5937–5942.
- 11 É. Lorenceau and D. Quéré, *J. Fluid Mech.*, 2004, **510**, 29–45.
- 12 F. Malik, R. Clement, D. Gethin, W. Krawszik and A. Parker, *Bioinspiration Biomimetics*, 2014, **9**, 031002.
- 13 K.-C. Park, P. Kim, A. Grinthal, N. He, D. Fox, J. C. Weaver and J. Aizenberg, *Nature*, 2016, **531**, 78.
- 14 D. Seo, J. Lee, C. Lee and Y. Nam, *Sci. Rep.*, 2016, **6**, 24276.
- 15 T. Nørgaard and M. Dacke, *Front. Zool.*, 2010, **7**, 23.
- 16 K. Zhang, F. Liu, A. J. Williams, X. Qu, J. J. Feng and C.-H. Chen, *Phys. Rev. Lett.*, 2015, **115**, 074502.
- 17 S. Haefner, O. Bäumchen and K. Jacobs, *Soft Matter*, 2015, **11**, 6921–6926.
- 18 J. B. Boreyko and C.-H. Chen, *Phys. Rev. Lett.*, 2009, **103**, 184501.
- 19 B. Carroll, *Langmuir*, 1986, **2**, 248–250.
- 20 B. J. Carroll, *J. Colloid Interface Sci.*, 1984, **97**, 195–200.
- 21 É. Lorenceau, C. Clanet and D. Quéré, *J. Colloid Interface Sci.*, 2004, **279**, 192–197.
- 22 G. McHale, N. A. Käb, M. I. Newton and S. M. Rowan, *J. Colloid Interface Sci.*, 1997, **186**, 453–461.
- 23 J. B. Boreyko and C.-H. Chen, *Phys. Fluids*, 2010, **22**, 091110.
- 24 F. Chu, X. Wu, B. Zhu and X. Zhang, *Appl. Phys. Lett.*, 2016, **108**, 194103.
- 25 N. Miljkovic, R. Enright, Y. Nam, K. Lopez, N. Dou, J. Sack and E. N. Wang, *Nano Lett.*, 2013, **13**, 179–187.
- 26 B. B. Sauer and T. E. Carney, *Langmuir*, 1990, **6**, 1002–1007.
- 27 Y. Nam, H. Kim and S. Shin, *Appl. Phys. Lett.*, 2013, **103**, 161601.
- 28 R. Enright, N. Miljkovic, J. Sprittles, K. Nolan, R. Mitchell and E. N. Wang, *ACS Nano*, 2014, **8**, 10352–10362.

29 L. Rayleigh, *Proc. London Math. Soc.*, 1879, **s1-s11**, 57–72.

30 P.-G. De Gennes, F. Brochard-Wyart and D. Quéré, *Capillarity and Wetting Phenomena*, Springer, 2004, pp. 33–67.

31 Z. Huang, Y. Chen, Y. Zheng and L. Jiang, *Soft Matter*, 2011, **7**, 9468–9473.

32 X. Li and Y. Peng, *Appl. Phys. Lett.*, 2006, **89**, 234104.

33 R. Mead-Hunter, B. J. Mullins, T. Becker and R. D. Braddock, *Langmuir*, 2010, **27**, 227–232.

34 D. Quéré, M.-J. Azzopardi and L. Delattre, *Langmuir*, 1998, **14**, 2213–2216.

35 L. Gao and T. J. McCarthy, *Langmuir*, 2006, **22**, 6234–6237.

36 R. E. Johnson Jr and R. H. Dettre, *J. Phys. Chem.*, 1964, **68**, 1744–1750.